

Integrated Clutter Cancellation and High-Resolution Imaging of Moving Targets in Multi-channel SAR

Diego Cristallini, Fabiola Colone, Debora Pastina, Pierfrancesco Lombardo

*INFOCOM Dept., University of Rome "La Sapienza"
Via Eudossiana, 18 – 00184 Rome, Italy*

Phone: +39 06 44585412 – Fax: +39 06 4873300

`{cristallini, fabiola.colone, debora, lombardo}@infocom.uniroma1.it`

Abstract— An integrated clutter cancellation and moving targets focusing scheme is presented for Multi-channel SAR (M-SAR) systems. The integration between the two processing steps is made feasible by performing the clutter cancellation processing in the Doppler frequency domain, and performing the moving target focusing by means of a bank of Chirp Scaling Algorithms (CSA). The integration results efficient from a computational point of view, since the azimuth FFT is common to both the clutter cancellation and the focusing processing. The clutter cancellation step allows to achieve sub-clutter moving targets visibility. The bank of CSA filters, each one matched to a different along-track target velocity component, allows to produce a high-resolution image of the target itself. The effectiveness of the proposed technique is shown with reference to a sample M-SAR dataset obtained from a SAREX-92 image.

I. INTRODUCTION

As it is well known, moving targets within SAR images appear shifted and/or smeared due to their motion [1]. In particular, an along-track target velocity component determines a variation in the resulting azimuth chirp rate and a consequent mis-match with the parameters used to focus the stationary scene, thus giving rise to target smearing. This target smearing determines a reduction in the achievable Signal to Clutter plus Noise Ratio (SCNR). This effect might deteriorate both the target detection capability and the imaging quality of movers. When only a single-channel SAR system is available, a viable solution to partially recover the detection capability is to design a more complex focusing algorithm which takes into account a possible along-track movement of the target, thus synthesizing several azimuth compression filters each one matched to a different relative along-track velocity between SAR sensor and moving target, as described in [2]. Since a high number of filters directly determines an increase in the computational cost, it is necessary to resort to a computational efficient focusing algorithm, like the Chirp Scaling Algorithm (CSA), [3]. This approach, presented in [4], allows to produce a high-resolution mis-located focused image of the movers.

However this SCNR recovery might not be sufficient for several environments, especially when sub-clutter moving targets visibility is required. In these cases, a Multi-channel SAR (M-SAR) system has to be considered, implementing either a Space-Time Adaptive Processing (STAP) scheme, [5], or an Along Track Interferometry (ATI) scheme, [6] and [7], for clutter cancellation before the bank of focusing filters. The

ATI-based approaches will not be taken into account in the following analysis, since, in these cases, an *a priori* information about the geometry is considered in the detection of the movers. On the other hand, when the motion direction of the movers is unknown, a viable clutter cancellation scheme resides in a STAP-based approach. Some possible implementations of STAP techniques applied to M-SAR systems have been addressed in [8] and [9]. In particular, in [8] a clutter cancellation scheme applied after FFT in the azimuth domain is presented. The main advantage of this approach is the asymptotical decoupling of the different Doppler frequency contributions if the time base is sufficiently long ([10]), which is the case of a M-SAR acquisition. This guarantees that the clutter cancellation can be performed separately for each Doppler frequency using only spatial Degrees Of Freedom (DOF).

In this paper we propose to merge the bank of CSA filters presented in [4] together with the clutter cancellation scheme in [8] to produce a high-resolution focused image of even very low Radar Cross Section (RCS) movers. A description of the resulting integrated clutter cancellation and focusing technique is reported in Section II. In Section III, the increased moving target detection capability is shown using as a case study a SAREX-92 image of the Tapajos rain forest with super-imposed synthetic returns from several moving targets. The performance of the proposed scheme is evaluated in terms of moving targets SCNR and azimuth resolutions improvements, while in Section IV we draw our conclusions.

II. INTEGRATED CLUTTER CANCELLATION AND BANK OF CSA

A block diagram of the integrated clutter cancellation and bank of focusing filters using the CSA is depicted in Figure 1 for the sample case of a three channels SAR system. As is apparent, the FFT in the azimuth domain required by the STAP technique is applied separated to the raw data acquired by each receiving channel. The azimuth FFT is also the first operation foreseen by the CSA, making feasible an efficient integration between the cancellation and the focusing steps. Once the clutter cancellation is performed, a bank of focusing filters is applied in parallel to the resulting clutter free data.

A. Clutter Cancellation in the Doppler Domain

STAP in the Doppler domain is a viable implementation in the M-SAR case. In fact, the echoes received from the stationary clutter can be modeled as a stationary process. It

can be demonstrated (e.g. [10]) that this assumption results in a frequency components decoupling of the clutter Fourier transform, if the time base is sufficiently long. This makes possible a clutter cancellation in each Doppler component using only the spatial DOFs, thus resulting in a small clutter plus noise covariance matrix to be estimated and inverted. Concerning the implementation of such a clutter cancellation scheme, two aspects have to be considered. First of all, the nice property of frequency components decoupling can be obtained only sampling the clutter signal in the azimuth domain at the Nyquist rate (i.e. PRF equal to the clutter Doppler bandwidth). Moreover the interference covariance matrices should be estimated on received data samples containing only clutter and thermal noise contributions (secondary data). In the following, such samples will be considered available to the system. It is worth to notice that this assumption is reasonable for the scenarios we are interested in. In fact, if the target received power is high with respect to the clutter plus noise contribution, a STAP approach might not be needed for adequate moving target detection, being sufficient only the SCNR recovery due to the bank of CSA. In contrast, a STAP approach is needed when the target received power is much lower than the clutter plus noise contribution. In this case, the interference covariance matrix can be directly estimated from secondary data samples containing target plus clutter plus noise contributions, being the target contribution negligible. A block diagram of the resulting cancellation scheme is reported in Figure 2 for the sample case of $M=3$ receiving channels.

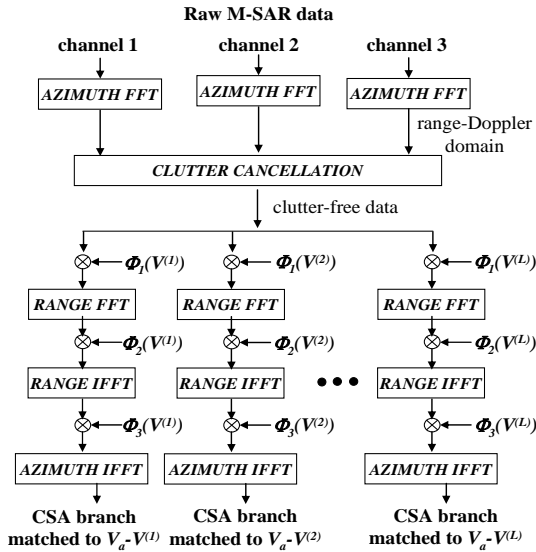


Fig. 1 – Integrated clutter cancellation and bank of CSA

The samples corresponding to the k -th row and to the n -th column of the matrices in the range-Doppler domain are collected in the $M \times I$ vector $\mathbf{x}_{k,n}$. The weight vector $\mathbf{w}_{k,n}$ is determined as:

$$\mathbf{w}_{k,n} = \hat{\mathbf{R}}_{k,n}^{-1} * \mathbf{s}_n, \quad (1)$$

where $\hat{\mathbf{R}}_{k,n}^{-1}$ is the inverse interference covariance matrix in the Doppler domain, estimated from P secondary samples adjacent in the fast-time direction to the k -th sample, and \mathbf{s}_n is a $M \times I$ vector accounting for temporal delay sampling on the different channels. The corresponding clutter-free sample $r_{k,n}$ is then obtained as:

$$\mathbf{r}_{k,n} = \mathbf{w}_{k,n}^H * \mathbf{x}_{k,n}. \quad (2)$$

As is apparent, a 3-DOFs nulling has to be performed separately for each Doppler frequency component and for each row of the uncompressed data, since the clutter may not be assumed stationary along the range dimension.

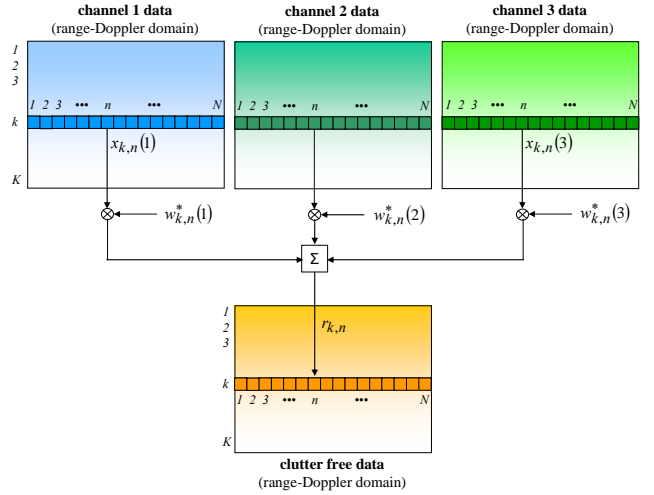


Fig. 2 – Clutter cancellation in the Doppler frequency domain

B. Bank of CSA

The focusing is based on a bank of L CSA, each one matched to a different possible target velocity component in the along-track (a.t.) direction. This means that in each CSA within the bank, the a.t. sensor velocity V_a has to be replaced with the relative a.t. velocity between sensor and target ($V^{(l)}$). Consequently, all the processing steps which depends on V_a have to be parallelized and customized, leading to the processing scheme sketched in Figure 1 (Φ_1 , Φ_2 , and Φ_3 are the phase multiplication terms of CSA).

The number of parallel branches L can be determined analytically by fixing a reasonable interval of target velocities and by knowing the overall synthetic aperture time, [2]. Each mover will be differently focused in the L images at the output of the L branches, showing a maximum peak level in the image obtained by using the a.t. velocity value that better approximates the relative a.t. velocity between target and sensor. A proper threshold (as for example obtained via a Cell Average CFAR) can then be applied to each output image to detect the movers.

C. Simplified bank of CSA

It is worth to notice that the first two phase multiplication terms foreseen by the CSA (i.e. Φ_1 and Φ_2) perform the Range Cell Migration (RCM) equalization and correction,

respectively. These two operations depend analytically on the relative a.t. velocity between SAR platform and moving target. However, from a practical point of view, given that the SAR platform velocity is much greater than the target a.t. velocity, the main contribution to target RCM is given by the SAR movement, while the a.t. movement of the target itself only gives a second order contribution to RCM¹. This consideration leads to a simplified processing scheme depicted in Figure 3.

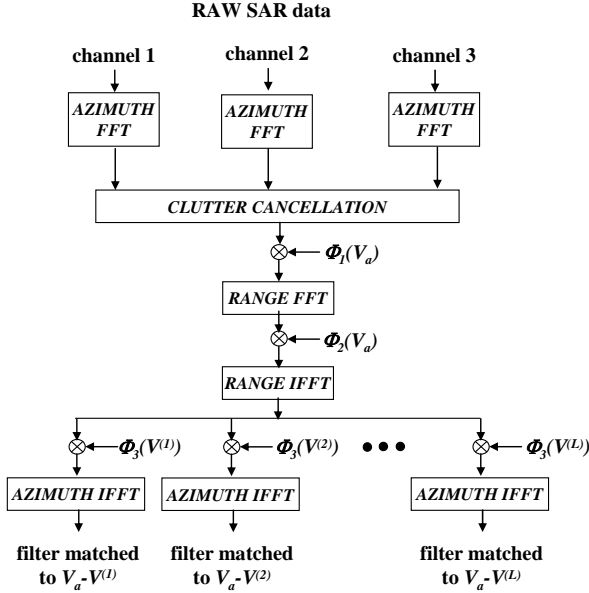


Fig. 3 – Integrated clutter cancellation and simplified bank of CSA

As is apparent, the RCM equalization and correction steps are performed neglecting the target movement in a.t.. Obviously, the target movement in along-track direction cannot be neglected in the third phase multiplication step, which performs the azimuth compression, hence this step has to be parallelized. The simplified processing scheme can be used with negligible degradation of moving targets imaging performance, if target a.t. velocity component does not yield additional RCM.

In the following is derived analytically the interval of a.t. target velocity component for which the simplified processing scheme cannot be applied, i.e. the interval of a.t. target velocity component causing additional RCM contribution. First of all, to formalize the additional RCM contribution due to target motion in a.t. direction, we refer to the sketch in Figure 4. Without loss of generality, we consider range compressed signals from three different targets (α , β , and γ) in the signal domain (fast time and slow time domain) and located at the same slant range.

In particular, target α has a positive a.t. velocity component (i.e. same direction of the SAR platform, $V_t > 0$), target γ has a

negative a.t. velocity ($V_t < 0$), while target β is stationary. As is apparent, all the targets experience the same slant range variation $\Delta R = R_{\max} - R_{\min}$. The difference in RCM behaviour is due to the different time intervals to move from R_{\max} to R_{\min} (i.e. the different dwell time intervals T_α , T_β , and T_γ). The target RCM contribution due to target motion in a.t. can be appreciated if and only if one of the following relation holds:

$$\begin{cases} \frac{T_\alpha}{2} - \frac{T_\beta}{2} \geq \frac{1}{PRF} & \text{for } V_t > 0 \\ \frac{T_\beta}{2} - \frac{T_\gamma}{2} \geq \frac{1}{PRF} & \text{for } V_t < 0, \end{cases} \quad (3)$$

that is, if the halved dwell time of a moving target differs from the halved dwell time of a stationary target (located at the same slant range) of a quantity greater than one pulse repetition interval. Assuming a flat earth geometry with the SAR trajectory parallel to the surface, the dwell time intervals can be expressed as:

$$\begin{cases} T_\beta = \frac{\lambda \cdot R_{\min}}{L_a \cdot V_a} & \text{stationary target} \\ T_\alpha = \frac{\lambda \cdot R_{\min}}{L_a \cdot (V_a - V_t)} & V_t > 0 \\ T_\gamma = \frac{\lambda \cdot R_{\min}}{L_a \cdot (V_a + V_t)} & V_t < 0 \end{cases} \quad (4)$$

where L_a is the antenna length in azimuth direction, and λ is the carrier wavelength. Substituting (4) in (3), one obtain

$$\begin{aligned} V_t > V_a - \frac{\lambda \cdot R_{\min} \cdot V_a \cdot PRF}{\lambda \cdot R_{\min} \cdot PRF + 2L_a \cdot V_a}, & \text{for } V_t > 0 \\ V_t < V_a - \frac{\lambda \cdot R_{\min} \cdot V_a \cdot PRF}{\lambda \cdot R_{\min} \cdot PRF - 2L_a \cdot V_a}, & \text{for } V_t < 0. \end{aligned} \quad (5)$$

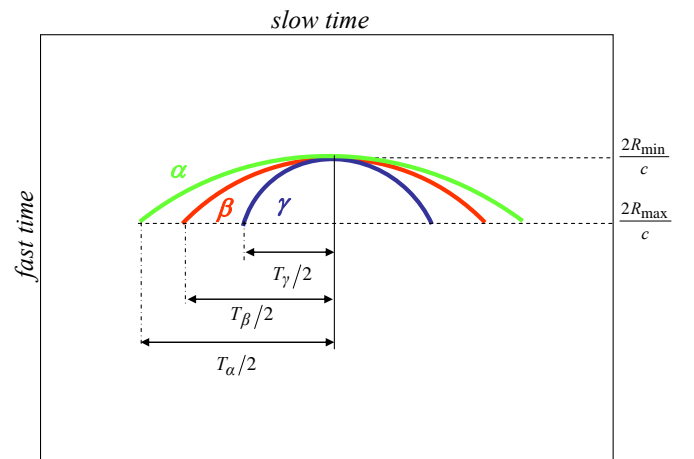


Fig. 4 – RCM behaviour for targets with different a.t. velocity components

¹ This is true only referring to the target velocity component in the a.t. direction. In fact, the assumption that the effect of radial target velocity on RCM (i.e. the range walk) can be neglected is much more restrictive, and might not be accepted, especially when dealing with very high resolution SAR. In this paper we will focus only to additional RCM due to a.t. target motion, while range walk effects will be opportunely compensated before processing.

Relations in (5) give the interval of V_i values that cause additional RCM. If (5) hold, the implementation of the *simplified bank of CSA* will give performance losses in imaging moving targets with respect to the *bank of CSA*. Depending on the scenario of interest, one may apply or not the simplified bank approach, making a trade off between imaging performance degradation and reduced computational cost, which is the main advantage of the simplified bank of CSA. To show this, in the following Table 1 a comparison of computational costs between the two approaches is reported. The computational burden is evaluated roughly in terms of multiplications and FFTs, assuming that the data have the same dimension in the range and azimuth domains.

The clutter cancellation step is not considered, since it is common to both approaches.

TABLE I
COMPUTATIONAL COST COMPARISON

	Phase Multiplications	FFTs
Bank of CSA	$3L$	$3L$
Simplified bank of CSA	$2+L$	$2+L$

III. CASE STUDY

To evaluate the effectiveness of the proposed technique, a M-SAR datacube of an observed scene with several moving targets is required. Unfortunately, the authors do not have access to a dataset with those characteristics. Therefore, an emulated M-SAR datacube has been derived starting from a SAREX-92 image of the Tapajos rain forest focused in the slant range-azimuth plane with a resolution of 6 meters, see Figure 5. To use such an input image for our purposes, we first applied an inverse focus processing to obtain the raw single-channel SAR data of stationary background. To do this, a flat Earth geometry has been supposed with the SAR working in non-squinted stripmap mode. Assuming the stationary background (i.e. clutter) to be perfectly correlated, a multi-channel SAR dataset can be derived from the single-channel SAR dataset by resampling the signal in the slow-time domain. In particular, the single-channel raw image has been first interpolated (i.e. over-sampled) and then properly decimated in the slow-time domain to obtain equivalent M-SAR raw data acquired from three receiving channels displaced in the along-track direction of a quantity dx and $2 \cdot dx$, respectively. The a.t. displacement dx has been chosen as $V_d/(3 \cdot PRF)$. In our first analysis neither an additional temporal decorrelation nor an additional spatial decorrelation has been added to the multi-channel clutter dataset. These three raw images have been added to thermal noise and to synthetic raw returns from several targets moving along roads A and B (see Figure 5). In particular, a Clutter to Noise Ratio (CNR_{RAW}) of 13 dB and a Signal to Clutter Ratio (SCR_{RAW}) of -28 dB (both measured on the single-channel raw data) have been considered. Figure 5 reports the focused image obtained combining coherently the three images and applying a CSA matched to the stationary background without any preliminary STAP processing step. After focusing, an averaged CNR_{FOC} of about 16 dB is experienced over the image. Moving targets

inserted in the image are represented by colored dots in their true position, an arrow indicating the corresponding motion. Circles of the same color indicate their smeared and displaced echo in the focused image.

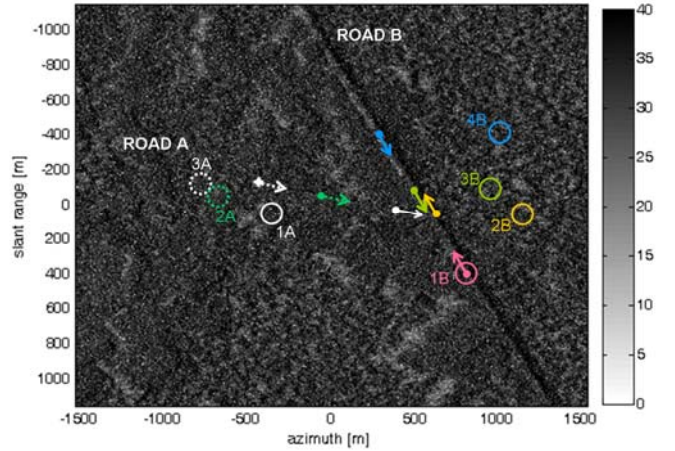


Fig. 5 - SAREX image with synthetic movers [dB]

Targets velocities and relative components in the radial and a.t. directions, are reported in Table 2. The maximum target velocity of 22 m/s has been selected considering the particular environment. For our study case we get a resulting number of filters $L=11$. Defocusing and low SCR_{RAW} make difficult target detection. It might be verified that for the considered scenario, relations in (5) do not hold, making feasible the implementation of the *simplified bank of CSA* for all the considered movers.

TABLE II
CONSIDERED TARGET VELOCITIES

Target	Velocity [m/s]	Radial component [m/s]	A.t. component [m/s]
1A (dark blue)	12	2.93	11.61
2A (green)	10	2.44	9.67
3A (red)	5	1.22	4.83
1B (purple)	-10	-8.78	-4.13
2B (yellow)	-22	-19.33	-9.10
3B (brown)	18	15.83	7.44
4B (light blue)	7	6.16	2.89

To show the effectiveness of the bank of CSA filters in correctly focusing moving targets, in Figure 6 we consider, as an example, the azimuth pulse response of target 2A when using the traditional CSA (i.e. with a.t. velocity given by the sensor velocity V_d), the *bank of CSA*, and the *simplified bank of CSA* (only the branch giving the maximum output power for the considered target). For simplicity, in this analysis neither clutter nor noise contributions have been added. As is apparent, a recovery in the peak target response as well as an improvement in the azimuth resolution is experienced. Moreover, the *simplified bank of CSA* matches the same imaging performance of the *bank of CSA*. Analogous results can be derived for all the considered targets.

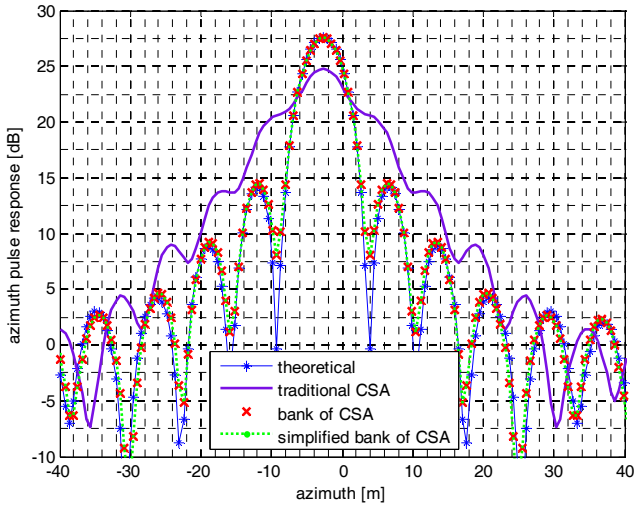


Fig. 6 – Comparison of azimuth pulse responses for target 2A

It is worth to notice that, in general, the target azimuth pulse response given by the bank of CSA might differ from the theoretical one obtained by using the exact value of the relative a.t. velocity between the sensor and the mover. A better approximation of the theoretical target pulse response could be possible increasing the number of branches, i.e. at the expense of a higher computational cost.

The same M-SAR raw datacube has been focused by means of traditional CSA with a preliminary STAP processing step after a range walk removal stage applied separately to each target. The 3×3 interference covariance matrices have been estimated on the basis of $P=6$ secondary data samples. The effectiveness of the clutter cancellation has been verified by measuring the reduction of the clutter plus noise power in the focused image with respect to the “no STAP case”, see Figure 5. In particular, a reduction of the clutter plus noise power close to 13 dB has been observed. This value is approximately equal to the maximum theoretical reduction, achievable when the clutter level is lowered down to the noise level (clutter plus noise power reduction = $\text{SCNR}_{\text{FOC}} - 3$ dB). In the first two columns of Table 3, the improvement in SCNR_{FOC} moving from the “no STAP case” to the “STAP case” can be appreciated, for a Monte Carlo simulation with 100 trials. As apparent, the SCNR_{FOC} improvement is lower than the clutter plus noise power reduction. This is mainly due to a reduction of the power signal level due to low target velocities. The resulting values of SCNR_{FOC} guarantee a proper target detection capability. Nevertheless, these returns appear still defocused, making the bank of CSA needed for high-resolution imaging. To show the effectiveness of the integrated processing, we still refer to target 2A. In particular, in Figure 7 a comparison among azimuth pulse responses is conducted for the following four cases: no STAP + traditional CSA, STAP + traditional CSA, STAP + *bank of CSA* processing, and STAP + *simplified bank of CSA*.

As is apparent, in the STAP + bank of CSA case, the target pulse response main-lobe becomes clearly visible against the interference background. Even in this case, the *simplified bank*

of CSA gives performance equivalent to the *bank of CSA*. An analysis of the SCNR_{FOC} achievable applying the integrated technique are reported in the third column of Table 3, referring to the Monte Carlo simulation mentioned above.

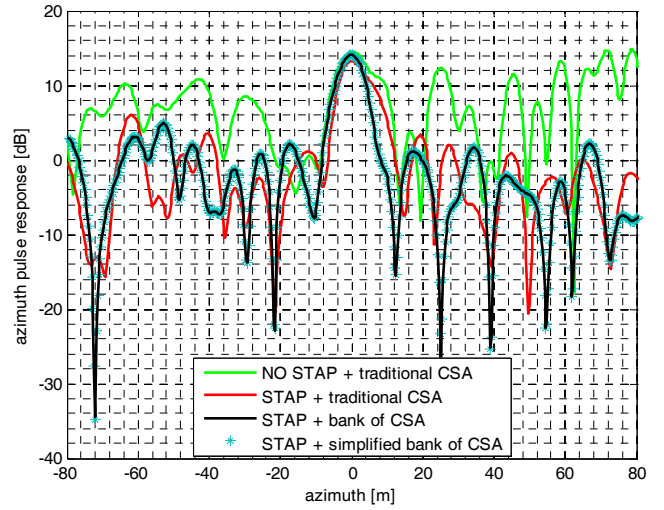


Fig. 7 – Comparison of azimuth pulse responses for target 2A

As expected, a further SCNR_{FOC} improvement is experienced applying the bank of CSA filters.

TABLE III
SCNR_{FOC} VALUES ON FOCUSED IMAGES

Target	NO STAP + traditional CSA	STAP + traditional CSA	STAP + bank of CSA
1A	4.6	14.6	16.5
2A	6.5	14.2	16.4
3A	6.7	15.7	16.1
1B	4.0	13.5	15.4
2B	3.5	12.1	15.2
3B	3.5	14.0	16.2
4B	5.5	14.7	15.5

In Table 4 is reported a comparison of azimuth resolutions (r_{AZ}) for the two cases of STAP + traditional CSA and STAP + simplified bank of CSA. As is apparent, an improvement in the achievable azimuth resolution is experienced for all the considered targets, making evident the need of the bank of CSA for high-resolution imaging of the movers.

TABLE IV
AZIMUTH RESOLUTIONS

Target	STAP + traditional CSA	STAP + simplified bank of CSA
	r_{AZ} [m]	r_{AZ} [m]
1A	13.9	9.2
2A	12.6	8.6
3A	10.4	9.4
1B	10.5	8.9
2B	11.9	8.5
3B	12.6	8.6
4B	9.9	9.2

Referring to the r_{AZ} values obtained applying the bank of CSA, two different aspects have to be considered. First of all, the bank of filters create a discretization of the possible moving targets azimuth chirp slopes. Secondly, the target radial velocity component might cause range walk, thus decreasing the dwell time and, consequently, the achievable azimuth resolution.

The application of the integrated technique to the available sample scenario shows that both steps (i.e. clutter cancellation and bank of focusing filters) are necessary for our purposes. The former allows to reduce the power level of stationary background making detectable the returns from moving targets, while the latter allows a correct imaging of the targets, recovering an acceptable azimuth resolution.

IV. CONCLUSIONS

An integrated technique for M-SAR clutter cancellation and high-resolution imaging of moving target has been presented. The clutter cancellation step is conducted in the Doppler frequency domain and the high-resolution focusing of movers is achieved by means of a bank of focusing filters based on a CSA approach. The proposed approach gives two main advantages. First of all, sampling at Nyquist rate in azimuth, clutter cancellation can be performed separately for each Doppler frequency using only spatial DOFs, resulting in small interference covariance matrices to be estimated and inverted. Moreover, the azimuth FFT required by this clutter cancellation technique is also the first operation required by the focus algorithm (i.e. the CSA). Hence this FFT is common to both the techniques, making feasible an efficient integration. Moreover a reduced cost focusing bank has been derived starting from the bank of CSA. Such an approach reduces the overall number of FFTs, neglecting the a.t. target motion in the RCM equalization and correction steps.

The effectiveness of the proposed integrated technique has been tested on a dataset with added synthetic moving targets.

ACKNOWLEDGMENT

This work has been funded by the Italian Ministry of University and Research under the FIRB project IMT-ARSEL.

REFERENCES

- [1] Raney R. K., "Synthetic aperture imaging radar and moving target", *IEEE Trans. AES*, 1971, **7**, pp. 499-505.
- [2] Barbarossa S., "Detection and imaging of moving objects with synthetic aperture radar, Part 1", *IEE Proc.-F*, 1992, **139**, (1), pp. 79-88.
- [3] Raney R. K., et alii, "Precision SAR processing using chirp scaling", *IEEE Trans. GRS*, 1994, **32**, (4), pp. 786-799.
- [4] Cristallini D., Lombardo P., Pastina D., "Chirp Scaling Based Detection of Moving Targets in SAR Images", *accepted to IGARSS 09*.
- [5] Klemm R., "Principle of Space-Time Adaptive Processing", IEE Publisher, 2002.
- [6] Weihing, D.; Hinz, S.; Meyer, F.; Suchandt, S.; Bamler, R., "An Integral Detection Scheme for Moving Object Indication in Dual-Channel High Resolution Spaceborne SAR Data," *Urban Remote Sensing Joint Event, 2007*, vol., no., pp.1-6, 11-13 April 2007.
- [7] Hinz, S.; Weihing, D.; Suchandt, S.; Bamler, R., "Detection and velocity estimation of moving vehicles in high-resolution spaceborne synthetic aperture radar data," *Computer Vision and Pattern Recognition Workshops, 2008*, vol., no., pp.1-6, 23-28 June 2008.

- [8] Ender J. H. G., "Space-time processing for multichannel synthetic aperture radar", *Electr. & Comm. Eng. Journal*, 1999, **11**, (1), pp.29-38.
- [9] Farina A., Lombardo P., "Space-time techniques for SAR", chapter in the book edited by Richard Klemm, "Applications of Space-Time Adaptive Processing", IEE Publisher, 2004.
- [10] Wei-Biao Wu, "Fourier Transforms of Stationary Processes", *Proc. of the American Mathematical Society*, vol. 133, no. 1, pp. 285-293.